Deconvolution of electron density from lithium beam emission profiles in high edge density plasmas

1993 Plasma Phys. Control. Fusion 35 1725

(http://iopscience.iop.org/0741-3335/35/12/006)

Plasma Phys. Control. Fusion 35 (1993) 1725–1744. Printed in the UK

Deconvolution of electron density from lithium beam emission profiles in high edge density plasmas

Z A Pietrzyk†, P Breger and D D R Summers
JET Joint Undertaking, Abingdon, Oxon, OX14 3EA, UK

Received 3 February 1993, in final form 24 May 1993

Abstract. Active beam emission spectroscopy with high energy Li beams has been shown to be a successful technique for determining electron density profiles of low and medium density plasma edges of a tokamak. For high density plasma edges, however, the reconstruction algorithm necessary to extract the electron density profile from the Li beam emission profile at 671 nm encounters a singularity point at which numerical instabilities can occur. This behaviour is particularly pronounced for noisy input data. An 'integral method' has been developed at JET to replace the standard calculation method in the singularity region of the profile, and the 'normal' deconvolution method is then used for data in the high density region. Using this approach, routine deconvolution of emission profiles extending from low density regions well into high density regions of the plasma has been made possible. The sensitivity of the algorithm to noisy input data and errors on input plasma parameters has been examined for typical conditions expected at JET. The simulations show that even for unfavourable conditions electron density profiles can be recovered with an overall accuracy better than 25%.

1. Introduction

Understanding plasma edge behaviour in a tokamak and substantiating existing edge models require measuring a wide range of plasma parameters (such as electron, ion and neutral densities, as well as their temperatures) with good spatial resolution over the entire scrape-off region. Furthermore, experimental evidence (McCormick *et al* 1992, Colton *et al* 1992) suggests that plasma confinement is affected by transport processes occurring on ms and sub-ms time scales. The implementation of edge diagnostic systems to supply such detailed information on the edge on a routine basis is thus of high priority. Profiles of the electron density and impurity concentrations will be measured at JET using an active Li beam diagnostic (Breger *et al* 1992). Profiles of electron densities have been measured successfully using Li-beam-emission spectroscopy (BES) in plasmas of low densities (below 10^{13} cm^{-3}) (Kadota *et al* 1978, McCormick *et al* 1984, 1985, 1987, 1989, 1992) and medium densities (a few 10^{13} cm^{-3}) (Schweinzer *et al* 1992a, Ueda *et al* 1992, Sasaki *et al* 1992, Wolfrum 1991, Wolfrum *et al* 1992). However, at JET high density plasmas with steep gradients near the last closed flux surface (LCFS) are achieved, and the extension of the method to steep edge gradients is required. For a successful application, the sensitivities of existing algorithms to experimental noise and numerical instabilities at higher densities need to be addressed. As the procedure

† CRPP Lausanne Switzerland.

0741-3335/93/121725 + 20 $07.50

used previously (McCormick *et al* 1987, McCormick *et al* 1989) required great numerical effort to deconvolute data from high-density plasmas, the development of a fast data analysis algorithm processing a large number of acquired profiles (of order 200 time slices) per pulse on an intershot basis, is needed. The dependence of the deduced density profiles on other (in general insufficiently well known) edge parameters has been reported (Wolfrum *et al* 1992). The beam attenuation is critically dependent on the impurity concentrations in the plasma edge. Using active charge-exchange radiation spectroscopy (CXRS), impurity profiles (Schorn *et al* 1991) have been measured using a high-energy Li-beam, and this technique will also be applied to the JET edge plasma to complement the existing impurity concentration measurements in the confined plasma region. The dependence of beam attenuation and emission calculations on a large number of plasma conditions means that a high degree of interaction of the electron density evaluation code with other diagnostic data is necessary. The concept of the diagnostic loop developed at JET (von Hellermann and Summers 1992) for the active CXRS in the confined plasma region needs to be extended to the edge. A new algorithm based on earlier work by one of the authors (ZAP) at ASDEX (McCormick *et al* 1987) has been developed at JET to cope with these demands.

2. The active beam method

Application of active beam emission spectroscopy for local plasma parameter determination has proven to be a very attractive diagnostic technique (Schweinzer *et al* 1992a, Schorn *et al* 1991, von Hellermann and Summers 1992, Breger *et al* 1991) since it can provide continuous, high-resolution measurements and it does not perturb the plasma. Light emitted from an injected particle beam (which is a direct indicator of the physical state of the beam) is related back to the plasma conditions along the beam trajectory. The relative order of transit time of the beam atoms through the light collection volume, the emission state lifetime and typical beam–plasma interaction times are critical in determining the complexity of analysis required and spatial resolution obtained. Whereas for many applications (e.g. large collection volumes (von Hellermann and Summers 1992)) the detected signal from a particular volume indicates the processes occurring in that *same* volume, the light collected from a high-energy Li beam at one position is an integral of all the processes along the beam trajectory preceding this position. To extract the desired density information a non-local deconvolution technique must be applied to the measured profile *as a whole.*

This deconvolution is characterized by several complications: a mathematical singularity occurs in the analysis equation (Schweinzer *et al* 1992a) (occurring at regions of high density typical for the JET plasma); there is a lack of accurate input information on beam current (Schweinzer 1991), temperature and impurity content of the plasma (Wolfrum *et al* 1992) and experimental data is noisy and of limited resolution. All these factors cause distortion in the solution.

In this paper we discuss an algorithm developed to deal with the numerical instabilities around the singularity point, thus allowing density evaluation well into the higher density plasma region. We also investigate the sensitivity of the algorithm to experimental factors.

Typically, a mono-energetic beam of neutral lithium atoms of 30 to 100 keV

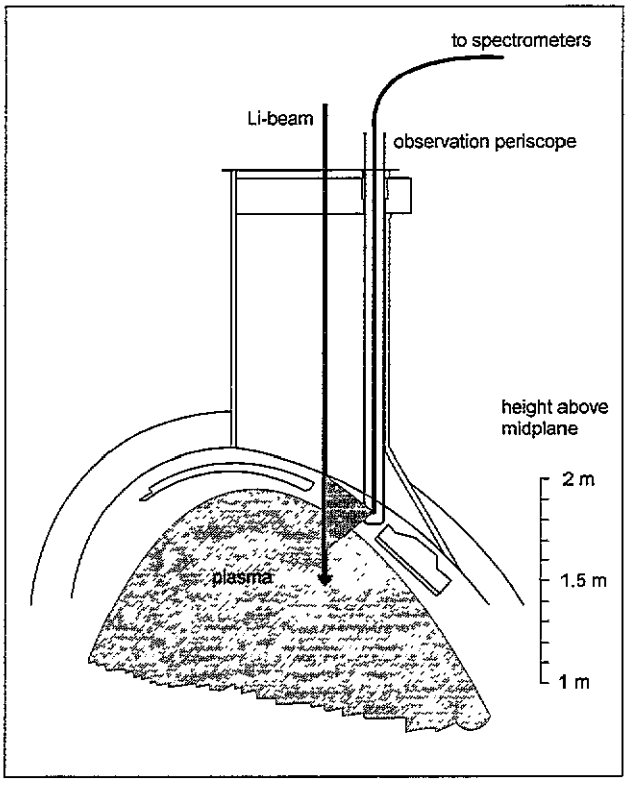

Figure 1. The Li beam injection system at JET. An observation periscope is employed to monitor the emitted radiation from a 20 cm section of the beam trajectory in the upper scrape-off-layer. The height above midplane indicated is used as x-axis coordinate in subsequent figures.

energy and intensity of 0.5–10 mA current equivalent is injected perpendicularly into the plasma edge. The Li I 2S-2P (6708 Å) resonance emission is recorded by optical imaging of the beam trajectory. Figure 1 shows a conceptual picture of the experiment as under construction on JET. The beam enters the plasma at a height of 2 m above the midplane, and encounters the LCFS at approximately 1.9 m above the midplane. The radial profile of emission is collected over a distance of 20 cm with a resolution of 5 mm. This emission is dependent on the atomic processes of excitation and ionization of the lithium atoms (see section 5 below). In this paper we will assume that the cross sections of these processes are sufficiently well known, and concern ourselves only with the algorithm of recovering the density distribution along the Li beam trajectory from the measured light intensity of 2S-2P transition.

The rate equations describing the atomic beam level populations can be written as

$$\frac{\mathrm{d}n_i}{\mathrm{d}t} = \sum_{j=1}^{n} (n_e n_j \alpha_{ij} + n_j \kappa_{ij}) \tag{1}$$

where n_e is the electron density, n_j are the atomic level population densities of the lithium atoms, α_{ij} are the collision rate coefficients, and κ_{ij} are the spontaneous emission coefficients. The mono-energetic lithium beam travels through the plasma

at velocity v_b, so the time-dependent variable can be transferred to the spatially-dependent variable (x denotes the beam penetration distance):

$$\frac{dn_i}{dt} = \frac{dn_i}{dx}\frac{dx}{dt} = v_b \frac{dn_i}{dx} \tag{2}$$

giving

$$\frac{dn_i}{dx} = \sum_{j=1}^{n} (n_e n_j a_{ij} + n_j k_{ij}). \tag{3}$$

These equations yield spatial distributions of $n_j(x)$, if $a_{ij}(x)$, $k_{ij}(x)$ and $n_e(x)$ are known. This procedure we will call *forward calculation* of the rate equations; it has been used to simulate the expected emission profiles for typical JET plasmas.

3. Evaluation algorithm

3.1. 'Normal' solution

In an experiment the value of $n_2(x)$ ($n_2 = 2P$ level population density) is inferred from the measured emission profile and $n_j(x)$ and $n_e(x)$ are unknown. To evaluate $n_e(x)$ a *reverse calculation* to the procedure described above is required. The second equation of system (3) can be written in the form:

$$\frac{dn_2}{dx} = n_e(x) \sum_{j=1}^{n} (n_j a_{2j}) + \sum_{j=1}^{n} (n_j k_{2j}) \tag{4}$$

from which the *exact* expression for $n_e(x)$ can be calculated:

$$n_e(x) = \frac{\dfrac{dn_2}{n_2\,dx} - \displaystyle\sum_{j=1}^{n} \left(\frac{n_j}{n_2} k_{2j}\right)}{\displaystyle\sum_{j=1}^{n} \left(\frac{n_j}{n_2} a_{2j}\right)}. \tag{5}$$

An important practical simplification is obtained by introducing the relative population densities (n_j/n_2) obviating the need for the absolute values of $n_j(x)$. In particular, $n_2(x)$ itself has the form of a logarithmic derivative which can be replaced by $dV_{ph}/V_{ph}\,dx$ where V_{ph} is the detector signal.

Using (5), $n_e(x)$ can be calculated only if all $n_j(x)/n_2(x)$ are known. In general, this is not the case, except at the beam's point of entry into the plasma, where to a good approximation all $n_j(x)$; $j > 1$ can be set to zero, i.e. the beam consists of ground-state atoms only. In practice, however, the first point observed on the emission profile is at some interior point x_0 in the plasma, where the boundary condition $n_1(x_0) + n_2(x_0) = n_{beam}$ is more appropriate. Then, the ratio $n_1(x_0)/n_2(x_0)$ can be obtained reliably from the two-level approximation

$$\frac{n_1(x_0)}{n_2(x_0)} = \frac{n_{beam}}{n_2(x_0)} - 1 \tag{6}$$

and n_{beam} needs to be known. A similar boundary condition may be invoked at some point in the plasma, where all neutral Li has been ionised, and from this the

beam intensity may be obtained if no singularity point is encountered in the profile range (Schweinzer *et al* 1992a). However, for most high-density emission profiles obtained, the singularity point position lies within the experimental range and a much more accurate value for the beam intensity can be inferred from the numerically stable behaviour of the algorithm at the singularity point.

The following numerical procedure is adopted to calculate $n_e(x)$. The rate equations (3) are solved using the Runge–Kutta method with $n_e(x)$ as calculated at the previous substep from equation (5) or (6) and known $V_{ph}(x)$ and $n_j(x)/n_2(x)$. If the measured signal is ideal (no noise and a very large number of input $V_{ph}(x)$ points) the procedure works well (see figure 2 in which the beam enters the plasma from the right). Simulated emission profiles are presented in this figure (calculated using equations (3) with a given $n_e(x)$) together with the $n_e(x)$ inferred using equation (5). In equation (5) both the numerator and denominator become zero simultaneously at some density and temperature. Physically, this corresponds to a state in the transient development of n_2 where the electron collision losses from level 2 are exactly balanced by electron collision gains. Since all electron collision rates are proportional to n_e, this condition is purely a function of the temperature (neglecting impurity ion and proton collisions)—no information on electron density can be gained at this spatial location. This condition is examined further in the analytical considerations in the appendix. It occurs at moderate densities of $2\text{–}3 \times 10^{13}\,\mathrm{cm}^{-3}$, and for many low-density tokamaks the emission profiles do not include the singularity point in their range. For higher densities, as expected in the JET plasma edge, this singularity point occurs in the middle of the interpretation region.

The mathematical singular point causes problems in numerical calculations, especially when one considers a real experimental case. The first unavoidable source of error is the finite experimental resolution, which is much larger than the required integration step of the order of 0.1 mm. The second imperfection occurs with the conversion of measured $V_{ph}(x)$ to $n_2(x)$. The emission collected at 670.8 mm will include plasma background radiation and detector noise. Even when minimized by proper experimental procedures, the remaining noise will cause numerical instabilities near the singularity. The ideal case of a singularity *point* is now replaced by a trajectory *range* which cannot be analysed in a 'normal' way. Slight deviations from precise values of $n_j(x)$ alter the position where the numerator and denominator cross zero. As a result, the calculated value of $n_e(x)$ becomes either negative or extremely large inside a singularity region.

3.2. *'Integral' solution*

There are several ways to solve the singularity problem in the numerical solution. The most straightforward method (McCormick *et al* 1984, 1987) uses the forward calculation near the singularity and assumes linear $n_e(x)$ dependence between experimental points. The calculation is repeated with different slopes of $n_e(x)$ and the result for which the calculated $n_2(x)$ from the rate equation agrees best with the experimental value is selected as a solution. The two disadvantages with this method are, first, that it is slow, and second, that the solution defined this way is not unique. Near the singularity two possible branches of solution exist: one with increasing and the other with decreasing density. A decrease in the level population $n_2(x)$ can be due either to reduced coupling to the ground state caused by a rapid decrease in

$n_e(x)$, or to an enhanced ionization attenuation of the overall level populations caused by a moderate increase of $n_e(x)$. Linear extrapolation of $n_e(x)$ to the next experimental point beyond the singularity position would give sufficiently close agreement with the measured $n_2(x)$ for positive as well as negative gradients to make a distinction between the two impossible. In conventional evaluations it is postulated that the density cannot decrease near the singularity point and a reasonable solution is obtained in most cases.

Here, we propose a different approach which is not based on an iterative method in the singularity region. Equation (4) can be integrated, giving

$$n_2(x) = \int_z^x n_e(x) \sum_{j=1}^{n} (n_j a_{2j})\, dx + \int_z^x \sum_{j=1}^{n} (n_j k_{2j})\, dx + n_2(z) \tag{7}$$

where z is the position at which the switch-over from the normal to the integral method is made. After integration by parts and rearranging one obtains

$$n_e(x) = \frac{n_2(x) + \int_z^x \frac{dn_e}{dy} \int_z^y \sum_{j=1}^{n} (n_j a_{2j})\, dx\, dy - \int_z^x \sum_{j=1}^{n} (n_j k_{2j})\, dx - n_2(z)}{\int_z^x \sum_{j=1}^{n} (n_j a_{2j})\, dx}. \tag{8}$$

In this last equation, the denominator is an integral of the denominator of equation (5), and thus does not go to zero at the singularity point. However, this solution requires knowledge of $dn_e(x)/dx$. In almost all points $dn_e(x)/dx$ can be supplied from the previous integration step in the same way as the population densities n_j, and thus the ambiguity in the sign of the slope may be avoided. However, near the singularity, such a procedure creates an unstable solution. Instead, in the new proposed method we supply $dn_e(x)/dx$ by calculating it *independently* at the approximate position of the singularity point. As this is a non-iterative approach, it also speeds up the deconvolution procedure.

3.3. Position and density at singularity

For a simple two-level system equation (5) becomes:

$$n_e(x) = \frac{\frac{dn_2(x)}{dx} - n_2(x)k_{22}}{n_1(x)a_{21} + n_2(x)a_{22}}. \tag{9}$$

At the singularity position both numerator and denominator are zero. Using the numerator, this condition yields the singularity position s:

$$\frac{dn_2(s)}{dx} = n_2(s)k_{22}. \tag{10}$$

As long as k_{22} is known this equation can be solved easily as $n_2(x)$ is directly related to the measured emission. The corresponding equation for a large number of levels

is as follows:

$$\frac{dn_2(s)}{dx} = \sum_{j=1}^{n} (n_j(s) k_{2j}). \tag{11}$$

In contrast to equation (10) this cannot be solved without first solving the system of differential equations (3) as no other $n_j(x)$ value except the input value $n_2(x)$ is known. In our algorithm we approximate this solution by assuming constant ratios of all $n_j(x)/n_2(x)$ between the last point calculated in the 'normal' way and the singularity. The results show that this assumption is valid in most cases.

To calculate the density $n_e(s)$ the first equation of system (3) can be used. As $n_2(s)$ and $dn_2(s)/dx$ are already known, we can use them to eliminate the unknown $n_1(s)$ from the first equation of system (3), assuming that the constants a_{ij} are not varying with x in this region. After mathematical transformation one gets for the two-level system

$$n_e(s) = \frac{\dfrac{a_{22}}{a_{21}} \dfrac{dn_2(s)}{dx} + k_{12} n_2(s)}{n_2(s)\left(a_{11} \dfrac{a_{22}}{a_{21}} - a_{12}\right)} \tag{12}$$

which can be extended to a multi-level system by assuming, as before, constant ratios of excited states. Hence

$$n_e(s) = \frac{C_1 \dfrac{dn_2}{dx} + n_2 B}{n_2 a_{11} C_1 - n_2 C_2} \tag{13}$$

where

$$C_1 = \frac{a_{22}}{a_{21}} + \sum_{3}^{n} \frac{a_{2j} n_j}{a_{21} n_2} \qquad C_2 = a_{12} + \sum_{3}^{n} a_{1j} \frac{n_j}{n_2} \qquad \text{and} \qquad B = k_{12} + \sum_{3}^{n} k_{1j} \frac{n_j}{n_2}.$$

3.4. Numerical procedure of $n_e(x)$ evaluation

We model the beam as a five-level system, i.e. in (3) $n = 5$. Using less levels causes significant errors in the predicted level population n_2. The use of more levels (including the $4s$–$4f$ levels) does not improve the accuracy of the method significantly (Schweinzer *et al* 1992a, Wolfrum 1991). As initial boundary condition we assume that all of the $n_j(0) = 0$ for $j > 2$. The population density $(n_1 + n_2)$ is calculated from the incident beam intensity. This measured intensity can be verified by cross-calibration of the diagnostic system with independent density measurements (Thomson scattering, Langmuir probes). With this assumption at the starting point x_0:

$$n_1(x_0) + n_2(x_0) = n_{\text{beam}} = \text{constant} \tag{14}$$

one obtains

$$\frac{n_1(x_0)}{n_2(x_0)} = \frac{n_{\text{beam}}}{n_2(x_0)} - 1$$

and from (9) one can calculate

$$n_e(x_0) = \frac{\dfrac{1}{n_2(x_0)}\dfrac{dn_2(x_0)}{dx} - k_{22}}{\left[\dfrac{n_{beam}}{n_2(x_0)} - 1\right]a_{21} + a_{22}}. \tag{15}$$

Integration is then started at this point. The integration step length in the Runge–Kutta method used to solve (3) is much smaller than the distance between the experimental points, so the measured $n_2(x)$ curve needs to be interpolated. Various methods of interpolation were tested, and the best results were obtained using a parabolic approximation. After each substep of the Runge–Kutta integration the density is calculated using the 'normal' method (5). When the value of the denominator falls below 10^{-8} the system switches to the 'integral' method (8). The population $n_2(0)$ in this equation is taken from $n_2(x_0)$ and $dn_e(x)/dx$ is calculated from the position and density at the singularity position and the last value of the 'normal' calculation. The advantage over the method used previously is that a single calculation replaces the iterative method, and the linear approximation of $n_e(x)$ is used only in one of the terms of (8) (i.e. the derivative of $n_e(x)$). The rest of the equation still uses the nonlinear dependence of $n_e(x)$. The system reverts to the 'normal' solution after crossing the singularity. Figure 2 shows examples of such

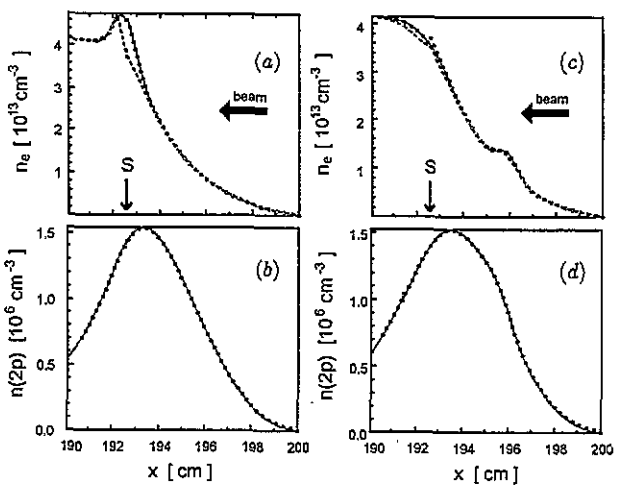

Figure 2. Typical results for two similar density profiles (figure 2(*a*) and 2(*c*)) with humps at different places. Figures 2(*b*) and (*d*) show the corresponding resonance emission profiles. The beam enters the plasma at 2 m above the midplane. The emission profiles (expressed as 2*p* population density) shown as solid lines are the result of the forward calculation using the density profiles shown in solid lines as input. The reverse calculation applied to these emission profiles yields the density profiles shown as dotted lines, which in turn would result in the emission profiles shown as dotted lines in a forward calculation. The profiles are calculated and deconvoluted with 5000 points. The dashed lines in figures 2(*a*) and (*c*) correspond to a deconvolution with 25 points, which corresponds to a typical experimental resolution. The beam energy is 60 keV and the effective neutral current is 1 mA with a beam width of 2 cm. *S* denotes the singularity point position in the profile.

calculations for profiles consisting of 25 experimental points in 10 cm distance. The profiles were selected to correspond to 'expected' JET scrape-off layer profiles, with additional humps of a Gaussian shape in two different locations. With these simulated ideal signals the reconstruction of $n_e(x)$ is very good indeed. Only small discrepancies occur near the hump and the singularity, related to the fact that the small number of points introduce an inaccuracy in the calculation (compare with the dotted curve which has a large number of points). Larger discrepancies occur where the hump is at the location of the singularity.

The process of deconvolution is sensitive to the incident n_{beam} specification (Schweinzer *et al* 1992a). This sensitivity is shown in figure 3 for three plasma profiles with different separatrix densities. The solid curves show correctly deconvoluted density profiles. If the incident beam intensity input to the reverse calculation is wrong by the percentage specified in the figure, the deconvoluted profile shown by the dotted curve is obtained. If the electron density is low (figure 3(*a*)) the sensitivity is not large, except near the singularity. If all the other parameters $a_{ij}(x)$ are known, this behaviour can be used to provide a more accurate determination of n_{beam} than

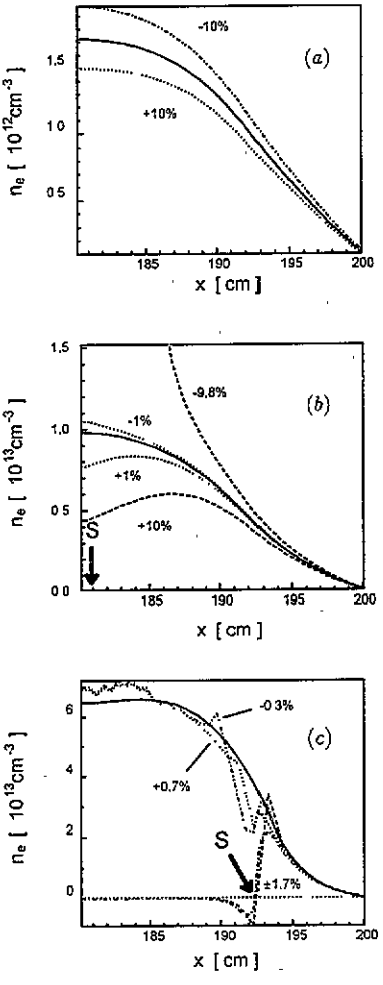

Figure 3. Effect of errors in specification of injected beam intensity to the deconvolution code. Density profiles of different separatrix density have been considered ((*a*), (*b*), (*c*)) showing increased sensitivity of the algorithm to incorrect beam specification with increasing density gradients. The beam energy is 60 keV and the effective neutral current is 1 mA with a FWHM of 2 cm. *S* denotes the singularity point position in the profile. At low density (*a*) no singularity point is encountered in the 20 cm profile length.

can be obtained from beam intensity measurements. Alternatively, if n_e near or behind the singularity is known, any other unknown input parameter to the algorithm in this region can be deduced (such as Z_{eff}).

4. Range of density profiles selected for performance testing

The stability behaviour of the deconvolution algorithm for different density profiles makes it possible to identify three electron density regimes. In the following the electron density profiles are to be characterized by the density n_{eo} reached at a position 10 cm into the plasma (with approximately exponential decay to the outside). The simplest and least sensitive to noise is the *low density range*, for which the $n_2(x)$ level population does not reach a maximum within the experimental range. It corresponds approximately to $n_{eo} < 10^{13}\,cm^{-3}$ and the 'normal' calculation method is sufficient. A *high density range* can be defined as a density for which the $n_2(x)$ signal is the same at the end of the experimental range as at the starting point. It corresponds to approximately $n_{eo} > 10^{14}\,cm^{-3}$. In this range it is also not difficult to deconvolute the density, since the singularity region is relatively small. Although there are larger errors in deconvolution near the singularity, the solution recovers very quickly. Between these two extremes of density gradients deconvolution is more difficult, the worst being cases where the singularity is close to the end of the experimental range. This occurs for densities $n_{eo} = 2\text{–}4 \times 10^{13}\,cm^{-3}$.

The 'typical' profile chosen for testing the performance of the algorithm is a profile which corresponds to a calculated scrape-off layer profile in JET with a divertor configuration. The beam is injected into a plasma edge at a position 2 m above the midplane and reaches the LCFS at about 1.9 m above the midplane. The density profile rises exponentially with exponent $0.417\,cm^{-1}$ and at the LCFS levels off to an internal density profile approximated here by a third-order polynomial. A small distortion of the profile using a hump of Gaussian form is added at various positions. Additional tests were done with low density and high density profiles. Figure 2 shows some of the profiles used for the test. In all calculations the neutral beam energy used is 60 keV and the temperature profiles rise exponentially with exponents of $0.307\,cm^{-1}$ to values at the LCFS of $T_e = 140$ eV and $T_i = 245$ eV. An equivalent neutral beam current of 1 mA has been used.

5. The coefficients in the rate equations

All of the above considerations assume that the coefficients $a_{ij}(x)$ and $k_{ij}(x)$ are known. Unfortunately, the coefficients $a_{ij}(x)$ are functions of electron and ion temperatures, and concentrations of impurity ions (Z_{eff}), which vary strongly across the scrape-off layer. As the respective profiles are not well known, and need to be specified to the analysis code as input, the sensitivity of the method to the assumptions made has to be tested.

Beam excitation and attenuation has to be calculated taking spontaneous

emission, electron, proton and impurity ion collisions into account. The collision processes included are excitation and de-excitation, direct ionization and charge exchange. The large number of cross sections coupling the five atomic levels have been obtained from various sources. All electron and proton collision cross-sections have been taken from a preliminary version (Schweinzer 1992) of a compilation of preferred data (Aumayr *et al* 1992). Charge exchange cross sections for impurity ion collisions have been estimated using a simple scaling formula by Janev (1991). The fit parameters necessary for this scaling formula have been calculated by comparison with data compiled by Aumayr and Winter (1987). For excitation and ionization collisions with impurity ions a simple q^2-scaling law has been used (Gilbody 1986). A detailed experimental programme to obtain more accurate atomic cross-section data is currently underway at the FOM-KVI, Groningen. Comparisons of the behaviour of our five-level code using this composite set of atomic data and simplified fit formulae (McCormick *et al* 1992, 1987, 1989) show good agreement as far as sensitivities to noise, temperature and Z_{eff} are concerned.

In order to include proton and ion collisions in the coefficients $a_{ij}(x)$ and $k_{ij}(x)$, the plasma dilution is modelled using the input specification of the density profiles of two impurity species (carbon and beryllium), as well as an average charge profile for both species. The diluted proton density n_{p} is calculated by the following approximation based on the plasma's quasi-neutrality (n_{C}, n_{Be} are the total impurity densities of all charge states q):

$$n_{\text{p}} \approx n_{\text{e}} - \frac{q^2_{\text{C,rms}} n_{\text{C}}}{6} - \frac{q^2_{\text{Be,rms}} n_{\text{Be}}}{4} \tag{16}$$

$$q_{k,\text{rms}} = \sqrt{\frac{\sum_{q=1}^{q_{\max}} q^2 n_{k,q}}{\sum_{q=1}^{q_{\max}} n_{k,q}}}. \tag{17}$$

The coefficients $a_{ij}(x)$ and $k_{ij}(x)$ are then calculated as follows:

$$\begin{aligned} a_{ij} &\equiv a_{ij}^{\text{el}} + \left(\frac{n_{\text{p}}}{n_{\text{e}}}\right) a_{ij}^{\text{p}} + \left(\frac{n_{\text{C}}}{n_{\text{e}}}\right) a_{ij}^{\text{C}} + \left(\frac{n_{\text{Be}}}{n_{\text{e}}}\right) a_{ij}^{\text{Be}} \\ a_{ij}^{k} n_k &\equiv \sum_{q=1}^{q_{\max}} \frac{\langle \sigma_{k,q} v \rangle}{v_{\text{b}}} n_{k,q} = q^2_{k,\text{rms}} \frac{\langle \sigma_p v \rangle}{v_{\text{b}}} n_k \end{aligned} \tag{18}$$

$$k_{ij} \equiv \begin{cases} 0 & \text{for } j < i \\ -\sum_{k<i} A_{ik}/v_{\text{b}} & \text{for } j = i \\ +A_{ji}/v_{\text{b}} & \text{for } j > i. \end{cases}$$

Here A_{ji} refers to the Einstein coefficients. The corresponding Z_{eff} is estimated at the end of the run for comparative purposes using the results for electron density:

$$Z_{\text{eff}} \approx \frac{n_{\text{p}}}{n_{\text{e}}} + \frac{n_{\text{C}}}{n_{\text{e}}} q^2_{\text{C,rms}} + \frac{n_{\text{Be}}}{n_{\text{e}}} q^2_{\text{Be,rms}}. \tag{19}$$

6. Performance tests of the reverse calculation

6.1. Sensitivity to signal noise

Experimental data contain statistical noise as well as detector noise, depending on the magnitude of the signal and the type of detector used. In this section we discuss a method to reduce the effect of noise on the accuracy of the reverse method, and discuss the error at different levels of noise. The noisy signals were simulated using the geometry of the JET Li beam system and typical performance figures of a CCD detector. An incident Li beam of 1 mA equivalent neutral current and 2 cm FWHM has been assumed throughout. An exposure time of 5 ms has been used to estimate the total noise level expected (read-out noise and electron statistical noise). It is typically ±2.5% deviation from the undisturbed signal, except for the low density wing of the signal profile where it becomes larger than ±5%. There may be additional noise from the plasma continuum radiation, which has to be subtracted from the total radiation to give the net signal for evaluation. To see the effect of larger noise levels, calculations with 10% and 15% noise level were also done.

Deconvolution of simulated data (typically 2.5% noise) without any noise reduction techniques is shown in figure 4. Various noise distributions were tested, all deconvoluted profiles were seen to lie within the error margin depicted by the light hatching in figure 4. The first 6–7 cm of the profile ($n_e(x) < 2 \times 10^{13}\,\mathrm{cm}^{-3}$) are insensitive to noise. At larger distances or higher densities the deviations due to noise become significant; at noise levels higher than 2.5% the signals could not be deconvoluted without additional noise-suppression techniques.

Several noise-reduction techniques have been tested, including polynomial fits to the measured emission profiles, Fourier transform spectral methods and weighted

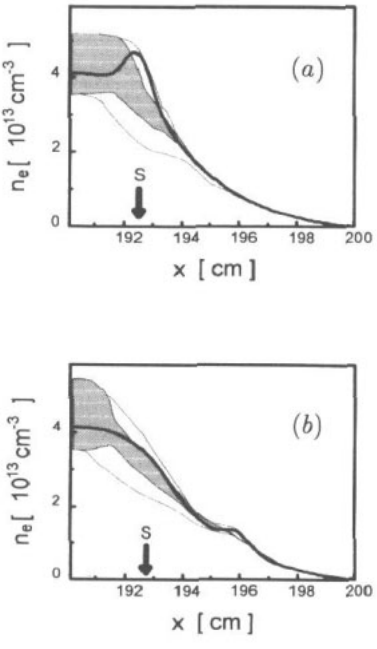

Figure 4. Deconvolution of the same profiles as in figure 2, with 25 experimental points, and ±2.5% statistical noise on the emission profiles. the two shaded bands show the range in which the deconvolved density profiles lie for different noisy profiles. The wide band shows the error range for deconvolved raw data, the narrow band shows the improvement obtained by introducing the noise reduction technique (Savitzky and Golay 1964). *S* denotes the singularity point position in the profile.

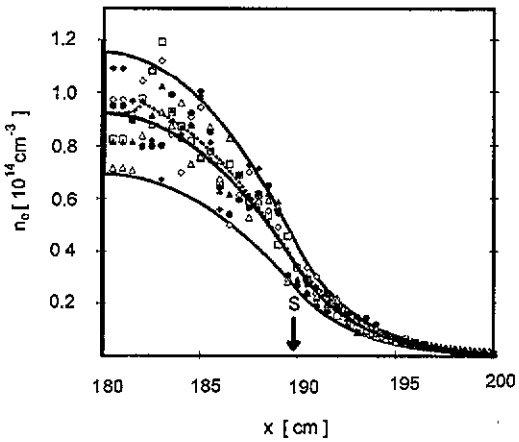

Figure 5. Deconvolution of emission profiles with ±15% statistical noise over a 20 cm range, with 40 experimental points. The noise reduction technique (Savitzky and Golay 1964) has been used. The solid curve and the bounded region show the true density profile and its ±25% error region. The dotted curve corresponds to the reconstructed electron density profile from an emission profile with limited experimental spatial resolution, but no noise. The various symbols correspond to reconstructed densities from emission profiles with different noise distributions. The results are seen to give the electron density profile with an error within the 25% margin. *S* denotes the singularity point position in the profile.

smoothing (Savitzky and Golay 1964). The weighted smoothing method based on least-sum square fitting of a parabola to several neighbouring experimental points (in our case seven points, three on each side of the experimental point) was found to be the most efficient for profiles of less than 100 experimental points. The results shown in this paper are based on this technique.

For noise levels of up to 2.5%, the improvements using this technique are only minimal, as shown in figure 4. It should be noted that a hump at 4 cm was also somewhat smoothed, but it can still be distinguished clearly from a simple exponential curve. The improvements obtained by the noise-reduction algorithm become apparent at noise levels higher than 2.5%, and for profiles extending up to 20 cm into the plasma. For 10% noise level, the density profile cannot be reconstructed without smoothing the data first. Similarly, as for the 2.5% noise level, the low density outboard profile is recovered very well, but deconvolution of higher density inboard sections of the profile is dependent on the noise distribution, in particular the signal distortion near the singularity. Generally, the main features of the profile are still recovered except in the last 2 cm where the smoothing does not occur. For comparison, the deconvolution of a signal with an even higher noise level of 15% over a 20 cm range is shown in figure 5. The smoothing technique has been employed. Using an experimental resolution of 5 mm the input density profile is reproduced very well over 16 cm. At this point the population levels have attenuated to below 1% of the incident beam density and the denominator in (5) is very small, leading to inaccuracy in the normal deconvolution procedure. The method employed is therefore switched to the 'integral' solution with $dn_e(x)/dx$ calculated from previous points. In practice this part of the data will have enhanced error bars as $n_2(x)$ becomes smaller than 1% of its maximum value and comparable to noise levels.

6.2. Sensitivity to electron and ion temperatures

The sensitivity of the rate coefficients to electron temperature is small since the beam energy (fixed here at 60 keV) is much larger than the local electron temperatures in the edge region. Changing the electron temperature by 50% does not change the solution outside the singularity region in the low density part of the profile. It effects deconvolution near the singularity and thus causes distortions inboard the singularity. Figure 6 shows profiles deconvoluted at the exact temperature and at temperatures ±50% of the temperature profile used to simulate the input signal. The corresponding error in the density profile is of the order of 10% and thus acceptable. These differences can be compensated for by small changes (of the order of 2%) in the incident beam intensity n_{beam}. Similar errors are obtained with respect to the ion temperatures. Since the solution in the singularity region is sensitive to changes of any parameter affecting the $a_{ij}(x)$ coefficients, profiles deconvoluted with high accuracy using the 'integral' method will still exhibit the largest error bar at the singularity.

6.3. Effect of impurity concentration and Z_{eff}

Impurity concentrations (or Z_{eff}) play a more important role than temperature in calculating the electron density profile. The charge exchange cross sections are strong functions of the impurity ion Z, whose concentration and charge states vary along the beam trajectory. To test the sensitivity of $n_e(x)$ to impurity concentrations we considered two impurities, beryllium and carbon, in the plasma. The calculation, as in the case of the temperature-dependence tests, is done by simulating the beam emission with prescribed profiles of impurity densities and charge states. The density distributions are then changed in the reverse calculation. In figure 7 a comparison is shown for a case when the input carbon densities to the deconvolution code are multiplied by a factor of 0.8, 1.2, 1.3 and 1.5 over the entire profile. From the graph one can see that a 30% change in the impurity concentration causes significant error near the singularity and a change by 50% prevents the deconvolution program crossing the singularity region.

Fortunately this extreme sensitivity exists near the singularity only. Near the plasma edge, where the impurity distribution is least known, the sensitivity is also least. This is shown in figure 8. Both impurity concentrations were changed by a factor of four at the edge, and near the singularity the impurity density profiles were changed so as to give a similar Z_{eff} (see figures 8(*b*), (*c*)). The resultant deconvolution (figure 8(*a*)) is almost perfect. To reinforce this point, further tests were done adding only carbon uniformly as well as non-uniformly over the profile (figure 9). Good reproduction of the original density profile is achieved despite large changes in the impurity concentration at the edge if the same Z_{eff} near the singularity is maintained. In the cases shown (figures 8 and 9), the plasma edge contains 30% impurities in the forward calculation and is almost entirely composed of impurities in the reverse calculation (a mixture of beryllium and carbon in figure 8 and only carbon in figure 9). This corresponds to Z_{eff} changes from 1.6 to 3.8 for figure 8 and from 1.4 to 4.6 for figure 9.

This high sensitivity to Z_{eff} changes near the singularity can in turn be used to advantage to measure Z_{eff} if the density near this region is independently known. Large differences between Z_{eff} in the plasma and that in the calculation will be signalled by a calculated electron density decreasing to zero (as in figure 7) or

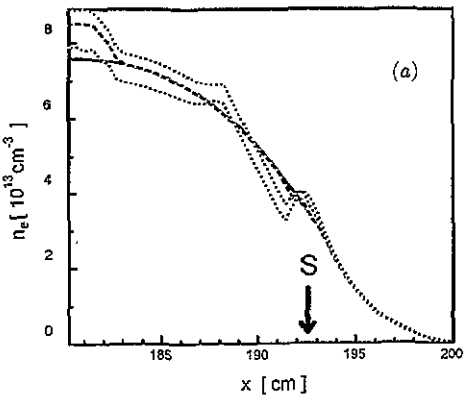

Figure 6. Sensitivity of deconvolution to electron temperature. (*a*) The emission profile was deconvolved at the correct temperature, and ±50% in temperature. The solid curve ——— denotes the input density, the dashed curve – – – – denotes the result of the reverse calculation at the correct electron temperature, and the dotted curves · · · · denotes the results of the reverse calculation at ±50% in temperature. *S* denotes the singularity point position in the profile. (*b*) The electron and ion temperature profiles used. The Li-beam energy is 60 keV.

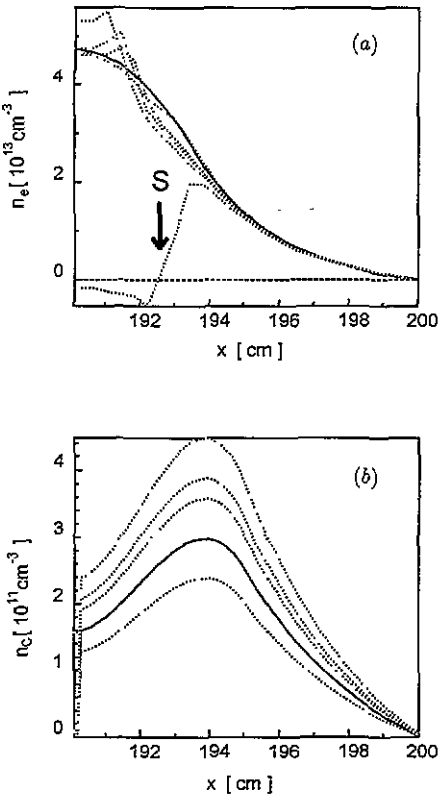

Figure 7. A case of impurity density change between forward and reverse calculation by a constant multiplier. (*a*) Density profiles deconvolved with different input specification of the concentration of carbon impurities. The solid curve corresponds to the correct specification, the dotted curves shows the deviations caused by erroneous impurity specification. *S* denotes the singularity point position in the profile. (*b*) The various concentrations of carbon specified to the deconvolution code. The solid line corresponds to the correct specification.

increasing to unrealistically high values in the singularity region. The input specification of complex impurity profiles to the deconvolution code is done by specification of a single characteristic Z_{eff} value. This pragmatic approach has been used successfully by Schweinzer *et al* (1992b).

7. Conclusions

We have described a technique of density evaluation from the 2S–2P emission of a lithium beam injected into the plasma. The method is not very sensitive to errors in temperature or impurity (Z_{eff}) profiles in the low density parts of the edge, and a technique similar to that previously used on ASDEX (McCormick *et al* 1984, 1987) can be employed. To extend the evaluation technique to the high-density region a

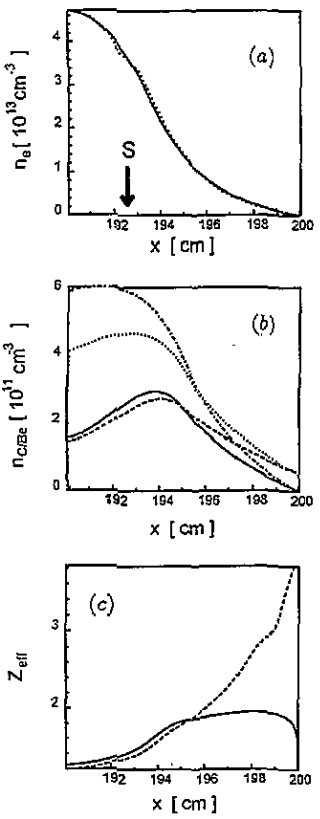

Figure 8. A case where both impurities are drastically changed between forward and reverse calculation at the plasma edge but Z_{eff} remains almost the same near the singularity region. (*a*) Density profiles deconvolved with different input specification of the concentration of carbon and beryllium impurities profiles. The solid curve ——— denotes the original input density, · · · · denotes the results of the reverse calculation with altered Z_{eff}. *S* denotes the singularity point position in the profile; (*b*) corresponding concentrations of carbon and beryllium specified to the deconvolution code, the solid curve ——— denotes the original carbon density, the dashed curve – – – – denotes the altered carbon density, the –·–·–· curve denotes the original beryllium density, and the dotted curve · · · · denotes the altered beryllium density; (*c*) Z_{eff} calculated from these concentrations, the solid curve ——— denotes the original Z_{eff}, and the dashed curve – – – – denotes the altered Z_{eff}.

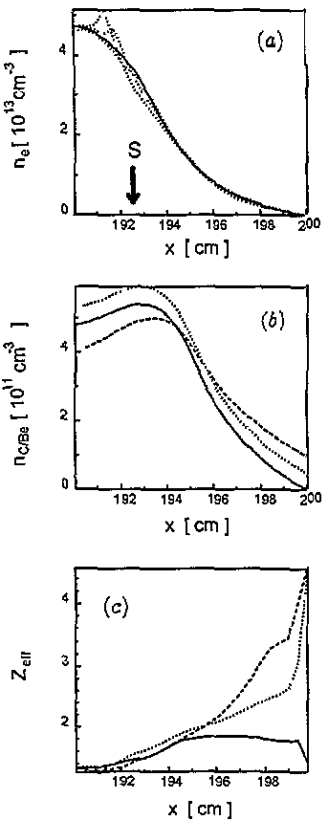

Figure 9. A case of single carbon impurity largely changed between forward and reverse calculation at the plasma edge but with the same and a slightly different Z_{eff} near the singularity. (*a*) Density profiles deconvolved with different input specification of the concentration of carbon density profiles. *S* denotes the singularity point position in the profile; (*b*) corresponding concentrations of carbon specified to the deconvolution code; (*c*) Z_{eff} calculated from these concentrations. The solid curves denote the original input quantities in the forward calculation, the dashed and dotted curves correspond to altered impurity densities during reverse calculations.

singularity region needs to be crossed. The integral method of deconvolution proposed provides an exact non-iterative method for this region. At plasma positions on *both* sides of the singularity region, the normal evaluation technique can be applied for density reconstruction.

The noise-reduction technique used here allows evaluation of noisy signals. In

general, no difficulty in deconvolution is encountered in regions where the electron density is below approximately $1 \times 10^{13}\,\mathrm{cm}^{-3}$ or above $4 \times 10^{13}\,\mathrm{cm}^{-3}$. Between these two regions, there is a singularity region (the exact position also depends on the density gradient and Z_{eff}) where the solution is very sensitive to small errors in the input data, such as noise, errors in Z_{eff}, temperature or incident lithium beam intensity. In extended regions of constant or almost constant electron density a sensitivity to small levels of noise similar to that near the singularity point is observed. Nevertheless, the electron density was seen to be recovered with an overall error not exceeding 25%.

If additional information on the electron density at any single point in the evaluation region is available, as for example from probe measurements or LIDAR measurements, the sensitivity of the evaluation method at the singularity region can be employed to estimate, for example, Z_{eff}. For some cases a very crude estimate can already be obtained by the requirement that the algorithm stays stable at the singularity point, with no further density calibration point. Apart from applying the BES method to the Li beam at JET, an active CXRS measurement of the dominant edge impurity ion will be performed as well. By combining the impurity content information from the Li-beam CXRS, the heating beam CXRS and various other impurity spectroscopic signals at JET, sufficiently well defined impurity profiles should be available as input data for the BES analysis code.

Acknowledgments

We are indebted to H Winter, J Schweinzer and their co-workers for communicating to us a preliminary release of their atomic database. Furthermore, we wish to thank K McCormick, R P Schorn and J Schweinzer for many helpful discussions, which benefitted the design of the JET Li beam diagnostic. This work was partially supported by the Swiss National Science Foundation.

Appendix. Analytical considerations

In this section, the analytical solution to the deconvolution problem is derived for the special case of a two-level system with constant coefficients, and the existence of the singularity as well as the behaviour of the solution near this point are examined.

For a simple two-level system equation (3) can be transferred to a second-order linear homogeneous differential equation:

$$\frac{\mathrm{d}^2 n_2}{\mathrm{d}x^2} - \left[n_{\mathrm{e}}(a_{11} + a_{22}) + k_{22} + \frac{1}{n_{\mathrm{e}}} \frac{\mathrm{d}n_{\mathrm{e}}}{\mathrm{d}x} \right] \frac{\mathrm{d}n_2}{\mathrm{d}x} - \left[n_{\mathrm{e}}^2 (a_{12}a_{21} - a_{22}a_{11}) + n_{\mathrm{e}}(k_{12}a_{21} - k_{22}a_{11}) - \frac{k_{22}}{n_{\mathrm{e}}} \frac{\mathrm{d}n_{\mathrm{e}}}{\mathrm{d}x} \right] n_2 = 0. \tag{A1}$$

With constant coefficients (i.e. for constant density and temperature) this equation can be solved analytically giving:

$$n_2(x) = C[\exp(\alpha_1 x) - \exp(\alpha_2 x)] \tag{A2}$$

where C is a constant related to the injected beam density n_{beam} and α_1 and α_2 are

two solutions of a quadratic equation:

$$\alpha^2 - \alpha[n_e(a_{11} + a_{22}) + k_{22}] - [n_e^2(a_{12}a_{21} - a_{11}a_{22}) + n_e(a_{21}k_{12} - a_{11}k_{22})] = 0. \tag{A3}$$

The analytical solution (A2) is very similar to the numerical solution for the five-level system with constant density but changing temperature. They are both characterized by a rapid increase of $n_2(x)$ followed by a slow decay. For the five-level system, the rate of increase is similar, whereas the decay rate is much faster than for the two-level system. This is to be expected, since the populating of higher-lying levels is larger at large distances x. It is interesting to note that for the case of constant density and temperature *there is no singularity* in either the two-level or the five-level system. This is apparent when considering the population ratio $n_2(x)/n_1(x)$, which becomes

$$\frac{n_2(x)}{n_1(x)} = -n_e a_{21}\left[(n_e a_{22} + k_{22}) + \frac{\alpha_1 \exp(\alpha_1 x) - \alpha_2 \exp(\alpha_2 x)}{\exp(\alpha_1 x) - \exp(\alpha_2 x)}\right]^{-1}. \tag{A4}$$

For large values of x this function converges to an asymptotic value of

$$R_x = \frac{n_2(x)}{n_1(x)} = \frac{-n_e a_{21}}{(n_e a_{22} + k_{22}) + \alpha_<} \tag{A5}$$

where $\alpha_<$ denotes the smaller of the two decay lengths $|\alpha_1|$, $|\alpha_2|$. As discussed above, the singularity occurs at s when the gains and losses through electron collisions balance exactly:

$$n_1(s)a_{21} + n_2(s)a_{22} = 0 \Rightarrow R_c = \frac{n_2(s)}{n_1(s)} = -\frac{a_{21}}{a_{22}}. \tag{A6}$$

For a multi-level system, the populations n_1 and n_2 dominate and the above value of ratio R_c will still be approximately valid. For a simple two-level system, and to a good approximation for a multi-level system, the ratio $n_2(x)/n_1(x)$ starts at the initial boundary condition and converges to R_x from below. If R_x is smaller than R_c then there is no singularity along the entire trajectory. As a_{22}, k_{22}, and $\alpha_<$ are negative coefficients, no singularity will occur in the two-level case for any value of constant electron density. The singularity condition corresponds to the asymptotic limit of electron collision processes dominating over all other population processes.

In the case of spatially varying density and temperature, the asymptotic population ratio R_x is no longer applicable, and the singularity position ratio R_c is now a function of distance. The population ratio at a particular point on the beam trajectory is determined by the preceding plasma conditions, whereas the singularity ratio R_c is a function of local plasma conditions. It is now possible for the ratio n_2/n_1 to exceed R_c. A necessary (but not sufficient) condition at this point is given by the requirement that the numerator of (10) becomes zero:

$$\frac{dn_2}{dx} = -|k_{22}|\, n_2 \Rightarrow n_2 = C \exp(-|k_{22}|\, x) \tag{A7}$$

showing that at least for the two-level case, as indeed also for most multi-level solutions, the singularity will always occur at a position beyond the emission profile

maximum. Substituting this into (13) yields for the density at the singularity

$$n_{e,crit} = \frac{k_{12}a_{21} + k_{22}a_{22}}{a_{11}a_{22} - a_{12}a_{21}}. \tag{A8}$$

As the coefficients a_{ij} are functions of atomic rates, beam energy, plasma temperature and impurity content, this electron density cannot be determined a priori, but estimates show that it typically lies near $n_{e,crit} = 2 \times 10^{13}$ cm^{-3}. Whether a singularity will occur at this density is then determined by the prevalent population density ratios, which are a consequence of the preceding plasma conditions as well as the injected beam state distribution.

For numerical reasons, the integral method introduced above must be applied over a range of x values where the denominator in equation (5) falls below a critical value R_s. The introduction of such a threshold effectively lowers the singularity criterion R_c to become

$$R_c = \frac{a_{21}}{|a_{22}| + R_s}. \tag{A9}$$

As a result, the integral method has to be used even for cases where the exact singularity point is not reached. It is interesting that numerically one can revert back to the normal method of deconvolution beyond the singularity for values of the denominator which are much smaller than R_S. In practice, the integral method is typically applied over a region where the denominator is

$$-R_s/100 \leqslant \sum_{j=1}^{n} n_j a_{2j} \leqslant R_s. \tag{A10}$$

References

Aumayr F and Winter H 1987 Atomic data base for lithium beam-activated plasma diagnostics IAP report 1/87, Technical University Vienna

Aumayr F, Janev R K, Schneider M, Smith J J, Schweinzer J, Wutte D and Winter H P 1992 Atomic data base for lithium beam edge plasma spectroscopy IAEA report INDC-NDS-267 (to be published)

Breger P, Xiao C and Kunze H-J 1991 *J. Phys. D: Appl. Phys.* **24** 2154

Breger P, Summers D and Vince J 1992 *Verhandlungen der Deutschen Physikalischen Gesellschaft* 5/92, 1357

Colton A L, Ali-Arshad S, Cripwell P and Porte L 1992 *10th International Conference on Plasma Surface Interactions 1992* Monterey

Gilbody H B 1986 *At. Mol. Phys.* **22** 143

Janev R K 1991 *Phys. Lett.* **160A** 67

Kadota K, Tsuchida K, Kawasumi Y and Fujita J 1978 *Plasma Phys. Control. Fusion* **20** 1011

McCormick K, Murmann H, El Shaer M and the ASDEX and NI Team 1984 *J. Nucl. Mater.* **121** 48

McCormick K and the ASDEX Team 1985 *Rev. Sci. Instrum.* **56** 1063

McCormick K, Pietrzyk, Z A, Murmann H, Lenoci M and ASDEX Team 1987 *J. Nucl. Mater.* **145** & **147** 215

McCormick K, Pietrzyk Z A, Sevillano E, Haas G, Murmann H D, Verbeek H and ASDEX Team 1989 *Controlled Fusion and Plasma Physics (Proc. 16-th Eur. Conf.* Venice **13b** part III European Physical Society p 895

McCormick K, Schweinzer J and Pietrzyk Z A 1992 *Controlled Fusion and Plasma Physics (Proc. 19th Eur. Conf.* Innsbruck) **16C** part II European Physical Society p 763

Sasaki S, Takamura S, Ueda M, Iguchi H, Fujita J and Kadota K 1992 National Institute for Fusion Science Report NIFS-147

Savitzky A and Golay M J E 1964 *Anal. Chem.* **36** 1627

Schorn R P, Hintz E, Rüsboldt D, Aumayr F, Schneider M, Unterreiter E and Winter H 1991 *Appl. Phys. B* **52** 71

Schweinzer J 1991 Lithium beam diagnostic at ASDEX upgrade *Symposium on Tokamak Edge Plasma Diagnostics by Injection of Lithium Atoms* Vienna

Schweinzer J 1992 private communication

Schweinzer J, Wolfrum E, Aumayr F, Pöckl M, Winter H, Schorn R P, Hintz E and Unterreiter A 1992a *Plasma Phys. Control Fusion* **34** 1173

Schweinzer J, McCormick K, Fiedler S, Aumayr F, Pöckl M and Winter H 1992b *Proc. 19th EPS Conf. Europhysics Conf. Abstracts* **16C** part II 1163

Ueda M, Iguchi H, Sasaki S, Fujita J and CHS group 1992 *J. Nucl. Mater.* **196–198** 923

von Hellermann M and Summers H P 1992 *Rev. Sci. Instrum.* **63** 5132

Wolfrum E 1991 Thesis, Technical University of Vienna

Wolfrum E, Schweinzer J, Schorn R P, Hintz E, Aumayr F and Winter H 1992 *Verhandlungen der Deutschen Physikalischen Gesellschaft* 5/92 1361